NASA-TM-111586

AIAA-96-1770

The Prediction of Ducted Fan Engine Noise Via a Boundary Integral Equation Method

M.H. Dunn and J. Tweed
Old Dominion University, Norfolk, Va.

F. Farassat
NASA Langley Research Center, Hampton, Va.

2nd AIAA/CEAS Aeroacoustics Conference
May 6-8,1996/State College, PA

For permission to copy or republish, contact the American Institute of Aeronautics and Astronautics 370 L'Enfant Promenade, S.W., Washington, D.C. 20024

THE PREDICTION OF DUCTED FAN ENGINE NOISE VIA A BOUNDARY INTEGRAL EQUATION METHOD

M. H. Dunn* and J. Tweed†
Old Dominion University
Norfolk, VA

F. Farassat‡
NASA Langley Research Center
Hampton, VA

Abstract

A computationally efficient Boundary Integral Equation Method (BIEM) for the prediction of ducted fan engine noise is presented. The key features of the BIEM are its versatility and the ability to compute rapidly any portion of the sound field without the need to compute the entire field. Governing equations for the BIEM are based on the assumptions that all acoustic processes are linear, generate spinning modes, and occur in a uniform flow field. An exterior boundary value problem (BVP) is defined that describes the scattering of incident sound by an engine duct with arbitrary profile. Boundary conditions on the duct walls are derived that allow for passive noise control treatment. The BVP is recast as a system of hypersingular boundary integral equations for the unknown duct surface quantities. BIEM solution methodology is demonstrated for the scattering of incident sound by a thin cylindrical duct with hard walls. Numerical studies are conducted for various engine parameters and continuous portions of the total pressure field are computed. Radiation and duct propagation results obtained are in agreement with the classical results of spinning mode theory for infinite ducts.

Notation

~	denotes that a quantity is dimensional when appearing over a variable
(r, ψ, z)	cylindrical coordinates - stationary frame
t	time
Z	axial coordinate - stretched, moving frame
$\tilde{r}_{max}$	maximum fan radius
$r_D^{\pm}$	radial coordinate of duct exterior (interior) profile
$\tilde{\rho}_0$	ambient density
$\tilde{c}$, c	ambient sound speed
V_F	forward flight speed
M_F	$= V_F/c$ forward flight Mach number
β	$= \sqrt{1-M_F^2}$ stretching parameter
N_B	number of fan blades
$\tilde{\Omega}, \Omega$	shaft speed
M_{TIP}	$= \tilde{r}_{max}\tilde{\Omega}/\tilde{c}$ tip Mach number
a	axial coordinate of duct trailing edge in stretched, moving frame
b	axial coordinate of duct leading edge in stretched, moving frame
L_D	ratio of duct length to duct diameter
m	circumferential mode number
k	$= mM_{TIP}$ characteristic wave number of m-th circumferential mode
k_z	axial wave number for first radial mode and m-th circumferential mode
κ	$= k/\beta$ modified wave number
p_t'	Eulerian description of total acoustic pressure field
p_s'	Eulerian description of scattered acoustic pressure field
p_i'	Eulerian description of incident acoustic pressure field
u_n	Eulerian description of normal component of acoustic velocity field
$\partial/\partial n$	normal derivative operator in stationary frame (with respect to outward facing normal to duct surface)
$\partial/\partial N$	normal derivative operator in stretched, moving frame (with respect to outward facing normal to stretched duct surface)
$\zeta^{\pm}$	surface acoustic impedance for duct exterior (interior)

---

* Research Associate Professor, AIAA Member
† Chairman, Department of Mathematics and Statistics
‡ Senior Research Scientist, AIAA Associate Fellow

Copyright © by the American Institute of Aeronautics and Astronautics, Inc. No copyright is asserted in the United States under Title 17, U.S. Code. The U.S. Government has a royalty-free license to exercise all rights under the copyright claimed herein for Governmental Purposes. All other rights are reserved by the copyright owner.

Introduction

Ducted fan engine noise is dominated by the fan component at takeoff and approach. Community exposure to the high levels of radiated fan noise at these conditions is significant. The reduction of tonal noise produced by the rotating components of high bypass turbofan engines is therefore of primary concern to the aeroacoustician. The design of active and passive noise abatement technology can be facilitated by advanced analytical tools for predicting the radiated sound from engine ducts. To be useful in design studies, prediction tools should be fast, versatile, accurate, and implementable on mainstream computer systems. The ability to compute only a portion of the sound field without the need to calculate the entire field is an important attribute in conducting rapid noise predictions. Computational approaches such as Finite Element Methods (FEM) and Computational Aeroacoustics (CAA) methods lack this property. For this reason, farfield noise calculations using FEM or CAA require vast amounts of computational time and computer storage. Therefore, the use of FEM and CAA for parametric studies in noise abatement research is limited.

In this paper, a Boundary Integral Equation Method for the prediction of ducted fan engine noise is presented. The method is based on the equations of linearized acoustics with uniform inflow. A scattering approach is adopted in which the acoustic pressure field is split into known incident and unknown scattered components. The source process is assumed to generate an incident pressure field that can be represented by a superposition of spinning modes. In a frame of reference moving with the engine duct and in regions of space not occupied by acoustic sources or scattering surfaces, the components of acoustic pressure are governed by Helmholtz' equation. An exterior boundary value problem is obtained by the inclusion of boundary conditions on the duct surfaces. The most general form of the boundary conditions allows for a spatially varying, locally reacting liner model on the duct surface.

By considering special values of the specific acoustic impedance in the boundary conditions, the classical Dirichlet and Neumann boundary values are obtained. The boundary value problem is then solved by expressing the scattered pressure field in terms of double and single layer Helmholtz potentials with unknown densities that are related to surface pressure and the normal derivative of surface pressure, respectively. Application of the boundary conditions to the layer representation yields a system of one-dimensional, hypersingular boundary integral equations for the unknown layer densities. The source terms for the system are related to the known incident pressure and its normal derivative. This system of boundary integral equations and method of solution comprise the BIEM.

The system of boundary integral equations is valid for engine ducts with arbitrary profile. If, however, the duct is approximated by an infinitesimally thin cylindrical tube, the complexity of the integral equation kernels is substantially reduced.

Analytical results will be presented that separate the singular and logarithmic portions of the integral equation kernels from the bounded parts. This analysis is significant because calculations involving singular and logarithmic integrals are available in closed form, thus avoiding time consuming, customized numerical integration techniques.

To demonstrate the BIEM, the solution procedure for a thin pipe geometry with hard wall boundary conditions is presented. A collection of spinning point dipoles located inside the duct are used to simulate the loading component of the fan noise and generate the incident pressure field. Several sets of engine operating parameters are considered in this study. Various researchers[1-5] have employed boundary integral techniques to solve this problem. Differences in the present work relative to the referenced works appear in the conclusions section of this paper.

Boundary Value Problem Derivation

In the analysis that follows, all quantities have been nondimensionalized; length by $\tilde{r}_{max}$, mass by $\tilde{\rho}_0 \tilde{r}_{max}^3$, and time by $\tilde{\Omega}^{-1}$.

We consider an engine fan surrounded by an axisymmetric, nondeformable duct of arbitrary profile translating in the +z (axial) direction with uniform speed V_F (see figure 1). The fan is composed of N_B equally spaced blades and rotates with shaft speed Ω. The incident acoustic pressure field generated by the fan is known. Linear conditions are assumed to apply and the inflow is uniform.

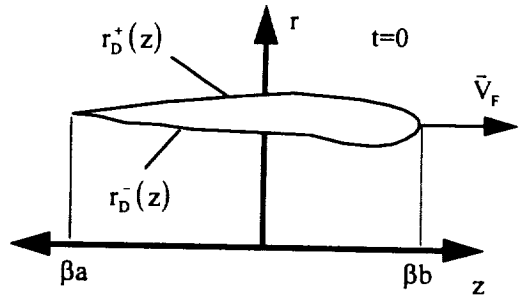

Figure 1: Duct Geometry
(Cylindrical, Stationary Coordinates)

Governing Differential Equations

The total acoustic pressure in the sound field is written as a sum of incident and scattered parts.

$$p_t'(r,\psi,z,t) = p_i'(r,\psi,z,t) + p_s'(r,\psi,z,t) \quad (1)$$

In regions of space that contain no scattering surfaces, p_s' is governed by the homogeneous wave equation.

$$\left[\frac{1}{c^2}\frac{\partial^2}{\partial t^2} - \frac{1}{r}\frac{\partial}{\partial r}\left(r\frac{\partial}{\partial r}\right) - \frac{1}{r^2}\frac{\partial^2}{\partial \psi^2} - \frac{\partial^2}{\partial z^2}\right]p_s' = 0 \quad (2)$$

Total acoustic pressure and acoustic velocity are related through the normal component of the acoustic momentum equation.

$$\frac{\partial u_n(r,\psi,z,t)}{\partial t} + \frac{\partial p_t'(r,\psi,z,t)}{\partial n} = 0 \quad (3)$$

In a frame of reference moving with the duct, all dependent acoustic variables can be expressed as linear superpositions of spinning modes. For example, the scattered pressure has the form

$$p_s'(r,\psi,Z,t) = \sum_{m/N_B=-\infty}^{\infty} P_s^m(r,Z)\, e^{im(\Omega t-\psi)} \quad (4a)$$

and the acoustic velocity is written

$$u_n(r,\psi,Z,t) = \sum_{m/N_B=-\infty}^{\infty} U_N^m(r,Z)\, e^{im(\Omega t-\psi)}, \quad (4b)$$

where the stretched, moving axial coordinate Z is given by

$$Z = \frac{z - V_F t}{\beta}. \quad (5)$$

The BIEM calculates modal amplitudes in (4) term by term. For notational convenience, the superscript m on the modal coefficients is dropped hereafter.

Define the dependent variables Q_s and Φ_N by

$$Q_s(r,Z) = P_s(r,Z)\, e^{i\kappa M_F Z} \quad (6a)$$

and

$$\Phi_N(r,Z) = U_N(r,Z)\, e^{i\kappa M_F Z}, \quad (6b)$$

with similar definitions for the total and incident pressures. Combining (4-6) with (2) yields the two dimensional Helmholtz equation

$$\left[\frac{1}{r}\frac{\partial}{\partial r}\left(r\frac{\partial}{\partial r}\right) + \frac{\partial^2}{\partial Z^2} - \frac{m^2}{r^2} + \kappa^2\right]Q_s = 0 \quad (7)$$

for the m-th coefficient. Using the definitions in (6), the momentum equation (3) can be written as

$$\Phi_N(r,Z) = \frac{1}{c} e^{i\frac{\kappa}{M_F}Z} \times \int_{-\infty}^{Z} e^{-i\frac{\kappa}{M_F}Z'}\left[\frac{\beta}{M_F}\frac{\partial Q_t}{\partial N'} - i\kappa M_F N_Z' Q_t\right]dZ', \quad (8)$$

where N_Z' is the axial component of the outward facing, unit normal to the stretched duct surface. Equation (8) is valid for $M_F > 0$. If the duct is stationary ($M_F = 0$), then (7) and (8) reduce to

$$\left[\frac{1}{r}\frac{\partial}{\partial r}\left(r\frac{\partial}{\partial r}\right) + \frac{\partial^2}{\partial z^2} - \frac{m^2}{r^2} + k^2\right]P_s = 0 \quad (9)$$

and

$$U_n(r,Z) + \frac{1}{ick}\frac{\partial P_t(r,Z)}{\partial n} = 0. \quad (10)$$

Equations (7-10) are valid for points not lying on the surface of the stretched duct.

Boundary Conditions

To meet noise certification levels it is necessary to treat the engine duct with passive noise suppression technology. In this work, the duct treatment is modeled by a locally reacting, axially varying liner.

Define the surface functions $Q_t^{\pm}$ and $\Phi_N^{\pm}$ by

$$Q_t^{\pm}(Z) = \lim_{r\to r_0^{\pm}(Z)} Q_t(r,Z) \quad Z\in[a,b] \quad (11a)$$

and

$$\Phi_N^{\pm}(Z) = \lim_{r\to r_0^{\pm}(Z)} \Phi_N(r,Z) \quad Z\in[a,b] \quad (11b)$$

with similar definitions for $Q_s^{\pm}$, $Q_i^{\pm}$, normal velocity, and all pressure components.

Myers[6] has shown that if $\zeta^{\pm}(Z)$ represents the specific acoustic surface impedance, then, in the stretched, moving frame of reference, the modal coefficients of velocity and pressure satisfy the boundary equation

$$\Phi_N^{\pm}(Z) + \left(1 + \frac{M_F^2}{\beta}\frac{\partial}{\partial Z}\right)\frac{Q_t^{\pm}(Z)}{\zeta^{\pm}(Z)} = 0 \quad Z\in[a,b]. \quad (12)$$

Equation (12) represents two boundary conditions, one for the exterior surface and the other for the interior surface. The boundary conditions for the stationary case reduce to

$$U_N^{\pm}(Z)+\frac{P_t^{\pm}(Z)}{\zeta^{\pm}(Z)}=0 \quad Z\in[a,b]. \tag{13}$$

By considering special values for the functions $\zeta^{\pm}$ in (12) and (13), several boundary conditions of interest are derivable. Total sound absorption is achieved if

$$\zeta^{+}=\zeta^{-}=\text{constant}\to 0. \tag{14}$$

Total sound reflection (hard walls) arises for

$$\zeta^{+}=\zeta^{-}=\text{constant}\to \infty. \tag{15}$$

Of particular relevance to actual engine ducts, is the case of a hard exterior surface ($\zeta^{+}\to\infty$) and lined interior. The boundary conditions for this situation are

$$\Phi_N^{+}(Z)=0 \quad Z\in[a,b] \tag{16a}$$

and

$$\Phi_N^{-}(Z)+\left(1+\frac{M_F^2}{\beta}\frac{\partial}{\partial Z}\right)\frac{Q_t^{-}(Z)}{\zeta^{-}(Z)}=0 \quad Z\in[a,b]. \tag{16b}$$

We now evaluate the momentum equation on the duct surface to obtain a relation between surface pressure and surface velocity. Let

$$\left(\frac{\partial Q_t}{\partial N}\right)^{\pm}(Z)=\lim_{r\to r_D^{\pm}(Z)}\frac{\partial Q_t(r,Z)}{\partial N}, \tag{17}$$

with normal derivatives of other dependent acoustic variables evaluated on the duct surfaces similarly defined. Then from (8), (10), and (11) we get

$$\Phi_N^{\pm}(Z)=\frac{1}{c}e^{i\frac{\kappa}{M_F}Z}\times$$

$$\int_{-\infty}^{Z}e^{-i\frac{\kappa}{M_F}Z'}\left[\frac{\beta}{M_F}\left(\frac{\partial Q_t}{\partial N'}\right)^{\pm}-i\kappa M_F N_Z' Q_t^{\pm}\right]dZ' \tag{18}$$

$$Z\in[a,b] \quad M_F>0$$

and

$$U_n^{\pm}(Z)=-\frac{1}{ick}\left(\frac{\partial P_t}{\partial n}\right)^{\pm}(Z). \tag{19}$$

$$Z\in[a,b] \quad M_F=0$$

Classical boundary conditions are obtained for the stationary case. Combining (13) and (19) yields the Robin's boundary conditions

$$\frac{P_t^{\pm}(Z)}{\zeta^{\pm}(Z)}-\frac{1}{ick}\left(\frac{\partial P_t}{\partial n}\right)^{\pm}=0 \quad Z\in[a,b]. \tag{20}$$

Dirichlet or Neumann conditions are obtained by application of (14) or (15), respectively, to (20).

We complete the derivation of the boundary value problem by requiring the dependent acoustic variables to satisfy the appropriate Sommerfeld radiation condition. Additional conditions may apply depending on the smoothness of the duct walls. If there are points on the duct that do not possess continuously turning tangent planes, then edge conditions specifying the behavior of the acoustic pressure at these points must be provided[7]. Edge behavior is determined from the physics of the problem together with an asymptotic analysis of the governing equations in a neighborhood of the edge. This problem occurs at the leading and trailing edges of the thin pipe approximation, for example.

Summary

The above analysis describes a uniquely solvable two dimensional boundary value problem for the scattered acoustic pressure in the sound field. For the stationary case, the boundary value problem is defined by (1), (9), (19), (20), the radiation condition, and the edge conditions (if applicable). If the duct is in motion, then (1), (6), (7), (12), (18), radiation and edge conditions completely define the boundary value problem.

Boundary Integral Equation Formulation

In this section, we reformulate the boundary value problem by deriving one dimensional boundary integral equations in which the boundary functions $Q_s^{\pm}$ and $Q_N^{\pm}$ are unknown, where

$$Q_N^{\pm}(Z)=\left(\frac{\partial Q_s}{\partial N}\right)^{\pm}(Z). \tag{21}$$

Once the scattered boundary functions are determined, the scattered pressure in the sound field is calculated pointwise via a Helmholtz layer representation that satisfies the Sommerfeld radiation condition implicitly.

Helmholtz Layer Representation

The Green's function for the two dimensional

Helmholtz operator in (7) can be written

$$G(r,r',Z-Z') = \frac{1}{2\pi}\int_0^{\pi} \cos m\psi \frac{e^{-ikR}}{R} d\psi \qquad (22)$$

where

$$R = \sqrt{r^2 + r'^2 - 2rr'\cos\psi + (Z-Z')^2}\,. \qquad (23)$$

Using results from Helmholtz potential theory[8] and (21-23), the solution of (7) is expressed as the sum of single and double layer Helmholtz potentials with densities $Q_N^{\pm}$ and $Q_s^{\pm}$, respectively. Thus,

$$Q_s(r,Z) = \mathbf{s}^+\left[Q_N^+\right](r,Z) - \mathbf{d}^+\left[Q_s^+\right](r,Z) + \mathbf{s}^-\left[Q_N^-\right](r,Z) - \mathbf{d}^-\left[Q_s^-\right](r,Z) \qquad (24)$$

Equation (24) is valid everywhere except for (r,Z) on the stretched duct surface. The field operators $\mathbf{s}^{\pm}$ and $\mathbf{d}^{\pm}$ are defined by

$$\mathbf{s}^{\pm}[f](r,Z) = \frac{1}{2\pi}\int_a^b f(Z')\left[\lim_{r'\to r_D^{\pm}(Z')} G\right] J^{\pm}(Z')dZ' \qquad (25)$$

and

$$\mathbf{d}^{\pm}[f](r,Z) = -\frac{1}{2\pi}\int_a^b f(Z')\left[\lim_{r'\to r_D^{\pm}(Z')} \frac{\partial G}{\partial N'}\right] J^{\pm}(Z')dZ' \qquad (26)$$

where f is some sufficiently smooth function and $J^{\pm}(Z')dZ'$ are the elements of arclength along the curves $r = r_D^{\pm}(Z')$.

If the boundary functions were known, then the scattered acoustic field could be obtained from (24).

Singular Boundary Operator Notation

In order to apply the boundary conditions to the field equation (24), it is necessary to evaluate the 2-D layer potentials and their derivatives on the stretched duct surface. The resulting 1-D boundary operators are singular. For $Z \in [a,b]$, define the following singular boundary operator - kernel pairs:

$$\mathbf{S}^{\pm}[f](Z) = \int_a^b f(Z')S^{\pm}(Z,Z')dZ'$$
$$S^{\pm}(Z,Z') = \frac{1}{2\pi}J^{\pm}(Z')\lim_{\substack{r'\to r_D^{\pm}(Z')\\ r\to r_D^{\pm}(Z)}} G \qquad (27)$$

$$\mathbf{D}^{\pm}[f](Z) = \int_a^b f(Z')D^{\pm}(Z,Z')dZ'$$
$$D^{\pm}(Z,Z') = \frac{1}{2\pi}J^{\pm}(Z')\lim_{\substack{r'\to r_D^{\pm}(Z')\\ r\to r_D^{\pm}(Z)}} \frac{\partial G}{\partial N'} \qquad (28)$$

$$\mathbf{S}_N^{\pm}[f](Z) = \int_a^b f(Z')S_N^{\pm}(Z,Z')dZ'$$
$$S_N^{\pm}(Z,Z') = \frac{1}{2\pi}J^{\pm}(Z')\lim_{\substack{r'\to r_D^{\pm}(Z')\\ r\to r_D^{\pm}(Z)}} \frac{\partial G}{\partial N} \qquad (29)$$

$$\mathbf{D}_N^{\pm}[f](Z) = \int_a^b f(Z')D_N^{\pm}(Z,Z')dZ'$$
$$D_N^{\pm}(Z,Z') = \frac{1}{2\pi}J^{\pm}(Z')\lim_{\substack{r'\to r_D^{\pm}(Z')\\ r\to r_D^{\pm}(Z)}} \frac{\partial^2 G}{\partial N \partial N'} \qquad (30)$$

$$\mathbf{S}_Z^{\pm}[f](Z) = \int_a^b f(Z')S_Z^{\pm}(Z,Z')dZ'$$
$$S_Z^{\pm}(Z,Z') = \frac{1}{2\pi}J^{\pm}(Z')\lim_{\substack{r'\to r_D^{\pm}(Z')\\ r\to r_D^{\pm}(Z)}} \frac{\partial G}{\partial Z} \qquad (31)$$

$$\mathbf{D}_Z^{\pm}[f](Z) = \int_a^b f(Z')D_Z^{\pm}(Z,Z')dZ'$$
$$D_Z^{\pm}(Z,Z') = \frac{1}{2\pi}J^{\pm}(Z')\lim_{\substack{r'\to r_D^{\pm}(Z')\\ r\to r_D^{\pm}(Z)}} \frac{\partial^2 G}{\partial Z \partial N'} \qquad (32)$$

Note that operators are denoted by bold face type. The kernels are singular for $Z - Z' = 0$. The nature of the singularities is examined below.

Singular Kernel Analysis

We list here, without proof, the asymptotic properties for $|Z-Z'| << 1$ of the above kernels. The singular character of the kernels is obtained by local analyses, the details of which will appear in a future publication:

$$S^{\pm}(Z,Z') = g_{13}^{\pm}(Z)\ln|Z-Z'| + K_1(Z,Z') \qquad (33)$$

$$D^{\pm}(Z,Z') = \frac{g_{22}^{\pm}(Z)}{Z-Z'} + g_{23}^{\pm}(Z)\ln|Z-Z'| + K_2(Z,Z') \qquad (34)$$

$$S_N^{\pm}(Z,Z') = \frac{g_{32}^{\pm}(Z)}{Z-Z'} + g_{33}^{\pm}(Z)\ln|Z-Z'| + K_3(Z,Z') \quad (35)$$

$$D_N^{\pm}(Z,Z') = \frac{g_{41}^{\pm}(Z)}{(Z-Z')^2} + \frac{g_{42}^{\pm}(Z)}{Z-Z'} + g_{43}^{\pm}(Z)\ln|Z-Z'| + K_4(Z,Z') \quad (36)$$

$$S_Z^{\pm}(Z,Z') = \frac{g_{52}^{\pm}(Z)}{Z-Z'} + g_{53}^{\pm}(Z)\ln|Z-Z'| + K_5(Z,Z') \quad (37)$$

$$D_Z^{\pm}(Z,Z') = \frac{g_{61}^{\pm}(Z)}{(Z-Z')^2} + \frac{g_{62}^{\pm}(Z)}{Z-Z'} + g_{63}^{\pm}(Z)\ln|Z-Z'| + K_6(Z,Z') \quad (38)$$

where $g_{ij}^{\pm}$, and K_i are known continuous functions.

The leading behavior for the single layer kernel (33) is logarithmic. Therefore, the associated operator is weakly singular. The leading terms for the kernels (34,35,37) are of the Cauchy type. Whilst, the kernels (36,38) are of the strongly singular Hadamard type. Consequently, integrals involved with the kernels (34-38) are divergent and must be interpreted in the finite part sense[10].

All of the above kernels have the logarithmic portions extracted. Integrations involving these terms are defined but difficult to achieve numerically. This problem is mitigated by the development of analytical results for the associated operators. Examples of this, as well as analytical results for the Cauchy and Hadamard terms, are presented in the results section.

Calculations involving the continuous portions of the kernels are performed by straightforward numerical integration.

Jump Relations from Potential Theory

Using the above operator notation, we state continuity properties for the single and double layers as a field point approaches the surface from the exterior of the duct. For sufficiently smooth f and $r_D^{\pm}$ (except possibly at $Z = a, b$), we have the following results[8] for $Z \in (a,b)$.

$$\lim_{r \to r_D^{\pm}(Z)} \mathbf{s}^{\pm}[f](r,Z) = \mathbf{S}^{\pm}[f](Z) \quad (39)$$

$$\lim_{r \to r_D^{\pm}(Z)} \mathbf{d}^{\pm}[f](r,Z) = -\frac{1}{2}f(Z) + \mathbf{D}^{\pm}[f](Z) \quad (40)$$

$$\lim_{r \to r_D^{\pm}(Z)} \frac{\partial}{\partial N}\mathbf{s}^{\pm}[f](r,Z) = \frac{1}{2}f(Z) + \mathbf{S}_N^{\pm}[f](Z) \quad (41)$$

$$\lim_{r \to r_D^{\pm}(Z)} \frac{\partial}{\partial N}\mathbf{d}^{\pm}[f](r,Z) = \mathbf{D}_N^{\pm}[f](Z) \quad (42)$$

Boundary Integral Equations

A system of integral equations for $Q_s^{\pm}$ and $Q_N^{\pm}$ is derived by applying the boundary conditions (12) and (18) to (24) and (39-42).

We begin by deriving some preliminary results. From (1), (6a), (11a), (24), and (39-40) we write

$$Q_t^{\pm}(Z) = Q_i^{\pm}(Z) + \mathbf{S}^{\pm}\left[Q_s^{\pm}\right](Z) + \left(\mathbf{I} - \mathbf{D}^{\pm}\right)\left[Q_N^{\pm}\right](Z) \quad Z \in [a,b] \quad (43)$$

and

$$\frac{\partial Q_t^{\pm}}{\partial Z}(Z) = \frac{\partial Q_i^{\pm}}{\partial Z}(Z) + \mathbf{S}_Z^{\pm}\left[Q_s^{\pm}\right](Z) + \frac{\partial Q_N^{\pm}}{\partial Z}(Z) - \mathbf{D}_Z^{\pm}\left[Q_N^{\pm}\right](Z) \quad Z \in [a,b] \quad (44)$$

Combining (1), (6a), (17), (24), and (41-42) yields

$$\left(\frac{\partial Q_t}{\partial N}\right)^{\pm}(Z) = \left(\frac{\partial Q_i}{\partial N}\right)^{\pm}(Z) + \left(\mathbf{I} + \mathbf{S}_N^{\pm}\right)\left[Q_s^{\pm}\right](Z) + \mathbf{D}_N^{\pm}\left[Q_N^{\pm}\right](Z) \quad Z \in [a,b] \quad (45)$$

Define the unknown surface vector functions $\bar{q}^{\pm}$ by

$$\bar{q}^{\pm}(Z) = \left(Q_s^{\pm}(Z), Q_N^{\pm}(Z)\right)^T. \quad (46)$$

Combining the boundary conditions (12) and (18) with results (33-46) yields the system of integral equations

$$\int_{-\infty}^{Z} e^{-i\frac{\kappa}{M_F}Z'} \mathbf{K}_1^{\pm}\left[\bar{q}^{\pm}\right](Z')dZ' + \mathbf{K}_2^{\pm}\left[\bar{q}^{\pm}\right](Z) = \bar{q}_i^{\pm}(Z) \quad Z \in (a,b) \quad (47)$$

for the four unknown surface functions. The vector function $\bar{q}_i^{\pm}$ is known from the incident pressure field and the integral operators $\mathbf{K}_1^{\pm}$ and $\mathbf{K}_2^{\pm}$ have the general form

$$\mathbf{A}(Z)\bar{q}^{\pm}(Z)+\mathbf{B}(Z)\frac{\partial\bar{q}^{\pm}(Z)}{\partial Z}+$$
$$\mathbf{C}(Z)\int_a^b\frac{\bar{q}^{\pm}(Z')}{(Z-Z')^2}dZ'+\mathbf{D}(Z)\int_a^b\frac{\bar{q}^{\pm}(Z')}{Z-Z'}dZ'+,\quad(48)$$
$$\mathbf{E}(Z)\int_a^b\bar{q}^{\pm}(Z')\ln|Z-Z'|dZ'+\mathbf{K}_B\left[\bar{q}^{\pm}\right](Z)$$

where $\mathbf{A},...,\mathbf{E}$ are matrices of known functions and $\mathbf{K}_B$ is an integral operator with continuous kernels. The matrix functions are determined from the coefficients in (33-38) and depend on the surface impedances and the duct curves $r=r_D^{\pm}(Z')$. Explicit expressions are lengthy and will not be presented here.

Examination of (48) indicates that (47) is a system of one dimensional, hypersingular, integro-differential equations of the second kind. As indicated previously, (47) must be augmented by a set of edge conditions if applicable. The authors are not aware of any theory that describes the solvability of (47). This subject is a matter of ongoing research. However, for certain simple cases, one of which is described in the next section, (47) is greatly simplified and solvability theorems do exist.

The characterization of the integral equation kernels by (48) greatly simplifies the numerical solution of (47). Analytical results for the logarithmic, Cauchy, and Hadamard kernels are available in many cases[11] and the continuous portions of the kernel can be computed by straightforward numerical integration.

Results

In this section, we consider the scattering of incident sound by an infinitesimally thin cylindrical duct of unit radius. The duct can be stationary or in motion. The interior and exterior walls of the duct are assumed to be hard. For this case, the complexity of the boundary integral equations is reduced significantly.

Boundary Integral Equation Formulation

From (12) and (18) the boundary conditions are

$$\int_{-\infty}^{Z}e^{-i\frac{\kappa}{M_F}Z'}\left(\frac{\partial Q_t}{\partial N}\right)^{\pm}(Z')dZ'=0\quad Z\in[a,b].\quad(49)$$

Differentiating (49) with respect to Z and using the relationships between total, scattered, and incident pressures yields the boundary equations

$$\left(\frac{\partial Q_t}{\partial N}\right)^{\pm}=Q_N^{\pm}\pm\left(\frac{\partial Q_i}{\partial r}\right)^{\pm}=0\quad Z\in[a,b].\quad(50)$$

Since the incident pressure and its derivatives are continuous across the duct surface we add the exterior and interior equations in (50) to get

$$Q_N^{+}+Q_N^{-}=0\quad Z\in[a,b].\quad(51)$$

Equation (51) is used below to simplify the field equation (24).

Define the jump in scattered pressure across the duct wall by

$$\Delta Q_s(Z)=Q_s^{+}(Z)-Q_s^{-}(Z)\quad Z\in[a,b].\quad(52)$$

Referring to (25-26) observe that

$$\mathbf{d}^{-}[f](r,Z)=-\mathbf{d}^{+}[f](r,Z)\quad(53)$$

and

$$\mathbf{s}^{-}[f](r,Z)=\mathbf{s}^{+}[f](r,Z).\quad(54)$$

Thus, applying (51-54) to (24) produces the field equation

$$Q_s(r,Z)=-\mathbf{d}[\Delta Q_s](r,Z).\quad(55)$$

Therefore, the scattered acoustic pressure in the sound field is written as a double layer with density given by the scattered pressure jump. Since the interior and exterior duct surfaces are the same, we have omitted the superscript on the double layer operator.

A single integral equation for ΔQ_s is obtained from (49) as follows: Use (42) to evaluate the normal derivative of (55) on the exterior wall, then combine this result with the exterior boundary condition in (49) to give

$$\int_{-\infty}^{Z}e^{-i\frac{\kappa}{M_F}Z'}\mathbf{D}_N[\Delta Q_s](Z')dZ'=$$
$$\int_{-\infty}^{Z}e^{-i\frac{\kappa}{M_F}Z'}\left.\frac{\partial Q_i}{\partial r}\right|_{r=1}(Z')dZ'\quad Z\in[a,b]\quad(56)$$

It is advantageous to rewrite (56) as the system of equations

$$\mathbf{D}_N[\Delta Q_s](Z)=\left.\frac{\partial Q_i}{\partial r}\right|_{r=1}(Z)\quad Z\in[a,b]\quad(57a)$$

and

$$\mathbf{g}[\Delta Q_s] = C_0. \tag{57b}$$

where the functional $\mathbf{g}$ is defined by

$$\mathbf{g}[f] = \int_{-\infty}^{a} e^{-i\frac{\kappa}{M_F}Z'} \mathbf{D}_N[f](Z')dZ' \tag{58}$$

and

$$C_0 = \int_{-\infty}^{a} e^{-i\frac{\kappa}{M_F}Z'} \left.\frac{\partial Q_i}{\partial r}\right|_{r=1} (Z')dZ'. \tag{59}$$

Equation (57a) is obtained by differentiating (56), and (57b) by evaluating (56) at the trailing edge. No information is lost by this reformulation. For the stationary case, (57b) is satisfied trivially. By performing a local analysis on the kernel in (57a) it can be shown to have the form

$$D_N(Z-Z') = \frac{A}{(Z-Z')^2} + B\ln|Z-Z'| + K_B(Z-Z'), \tag{60}$$

where A and B are known constants and the kernel K_B is continuous and simple to evaluate numerically.

To obtain a unique solution to (57a,b), the behavior of the pressure jump at the duct leading and trailing edges is required. It is known that the jump in pressure has the following asymptotic behavior:

$$\Delta Q_s = \begin{cases} O\left(\sqrt{Z-a}\right) & Z \to a^+ \\ O\left(\frac{M_F}{\sqrt{b-Z}} + \sqrt{b-Z}\right) & Z \to b^- \end{cases}. \tag{61}$$

Based on (61) we assume a solution of the form

$$\Delta Q_s(Z) = \alpha\sqrt{\frac{b-Z}{Z-a}} + \sqrt{(b-Z)(Z-a)}\,\gamma(Z), \tag{62}$$

where α is an unknown constant and γ is an unknown continuous function. Note that if the duct is stationary, then $\alpha = 0$.

A method is now developed in which the determination of γ is separated from the calculation of α. This yields an integral equation for γ that is relatively simple to solve. Use (62) in (57b) to obtain

$$\alpha = \frac{C_0 - \mathbf{g}^{(1/2,1/2)}[\gamma]}{\mathbf{g}^{(1/2,-1/2)}[1]}, \tag{63}$$

where

$$\mathbf{g}^{(\eta,\xi)}[f] = \mathbf{g}\left[(Z-a)^\eta (b-Z)^\xi f\right]. \tag{64}$$

The notation in (64) will be used with other integral operators in the remainder of this analysis. Substituting (62-62) in (57a) gives the first kind integral equation

$$\mathbf{K}^{(1/2,1/2)}[\gamma](Z) = q(Z) \quad Z \in [a,b], \tag{65}$$

where

$$\mathbf{K}^{(1/2,1/2)}[\gamma](Z) = \mathbf{D}_N^{(1/2,1/2)}[\gamma](Z) - \frac{\mathbf{g}^{(1/2,1/2)}[\gamma]}{\mathbf{g}^{(1/2,-1/2)}[1]}\mathbf{D}_N^{(1/2,-1/2)}[1](Z) \quad Z \in [a,b] \tag{66}$$

and

$$q(Z) = \left.\frac{\partial Q_i}{\partial r}\right|_{r=1}(Z) - \frac{C_0}{\mathbf{g}^{(1/2,-1/2)}[1]}\mathbf{D}_N^{(1/2,-1/2)}[1](Z) \quad Z \in [a,b]. \tag{67}$$

The kernel for the operator in (66) has the same form as (60). After solving (65) for γ, (63) is used to calculate α.

Numerical Solution

Due to the edge behavior associated with γ, it is natural to expand γ in a series of Chebyshev polynomials of the second kind. Thus, constants $\{\gamma_j\}_{j=0}^{\infty}$ are sought such that

$$\gamma(Z) = \sum_{j=0}^{\infty} \gamma_j U_j\left(\frac{2Z-a-b}{b-a}\right), \tag{68}$$

where

$$U_j(x) = \frac{\sin\left[(j+1)\cos^{-1}x\right]}{\sin\left(\cos^{-1}x\right)}. \tag{69}$$

Golberg[9] has shown that if κ is not an eigenfrequency of $\mathbf{K}$, then a unique convergent expansion such as (68) exists for integral equations with kernels of the type given in (60).

To solve (65) numerically, we truncate the expansion in (68) and apply the collocation method. Other popular projection techniques, such as Galerkin's method, require an additional numerical integration relative to collocation. With proper choice of collocation points and numerical quadrature scheme for the continuous portion of the kernel, Golberg[9] has shown that the accuracy obtained by Galerkin's method and collocation are equivalent for this problem. Thus, collocation yields the same accuracy as Galerkin's method, but with substantially less computational work.

The numerical solution begins by choosing the number of terms in the expansion (68), N_0+1. This number is a function of the modified wave number κ. If $\bar{\gamma}$ denotes the approximate solution, then

$$\bar{\gamma}(Z)=\sum_{j=0}^{N_0}\gamma_j U_j\left(\frac{2Z-a-b}{b-a}\right). \tag{70}$$

The collocation points, $\{Z_j\}_{j=1}^{N_0+1}$ are given by the zeroes of the N_0+1-th Chebyshev polynomial of the first kind and the numerical integration scheme for the continuous kernel is chosen as Gauss quadrature with weights and nodes based on second kind Chebyshev polynomials. Evaluating (65) at the collocation points yields the linear system

$$\sum_{i=0}^{N_0}\gamma_i \mathbf{K}^{(1/2,1/2)}[U_i](Z_j)=q(Z_j), \qquad j=1,\ldots,N_0+1 \tag{71}$$

for the unknown expansion coefficients. The invertibility of the linear system has been established by Golberg.

To compute (71), integrals of the type

$$\int_{-1}^{1}\frac{\sqrt{1-x'^2}\,U_j(x')dx'}{(x-x')^2} \qquad x\in(-\infty,1], \tag{72}$$

$$\int_{-1}^{1}\sqrt{1-x'^2}\,U_j(x')\ln|x-x'|dx' \qquad x\in(-\infty,1], \tag{73}$$

$$\int_{-1}^{1}\sqrt{\frac{1+x'}{1-x'}}\frac{dx'}{(x-x')^2} \qquad x\in(-\infty,1], \tag{74}$$

and

$$\int_{-1}^{1}\sqrt{\frac{1+x'}{1-x'}}\ln|x-x'|dx' \qquad x\in(-\infty,1], \tag{75}$$

are encountered. Analytical results are obtained for (72-75) by applying the Plemelj-Sokhotski theorem[7] and its logarithmic analog to the complex function

$$R_j(w)=\left[w-\left(w^2-1\right)^{1/2}\right]^j$$

with branch cut

$$|\mathrm{Re}(w)|<1 \quad \mathrm{Im}(w)=0.$$

The branch is defined such that $\left(w^2-1\right)^{1/2}$ is real and positive if w is real and greater than one. This analysis yields the following results:

$$\int_{-1}^{1}\frac{\sqrt{1-x'^2}\,U_j(x')dx'}{(x-x')^2}=-\pi(j+1)\times \begin{cases} U_j(x) & x\in[-1,1] \\ \dfrac{\left(x+\sqrt{x^2-1}\right)^{j+1}}{\sqrt{x^2-1}} & x<-1 \end{cases}, \tag{76}$$

$$\int_{-1}^{1}\sqrt{1-x'^2}\,U_0(x')\ln|x-x'|dx'= \frac{\pi}{2}\begin{cases} \dfrac{1}{2}T_2(x)-\ln 2 & x\in[-1,1] \\ \dfrac{1}{2}\left(x+\sqrt{x^2-1}\right)^2+ \\ \quad \ln\left(-x+\sqrt{x^2-1}\right) & x<-1 \end{cases}, \tag{77}$$

$$\int_{-1}^{1}\sqrt{1-x'^2}\,U_j(x')\ln|x-x'|dx'= \frac{\pi}{2}\begin{cases} \dfrac{T_{j+2}(x)}{j+2}-\dfrac{T_j(x)}{j} & x\in[-1,1] \\ \dfrac{\left(x+\sqrt{x^2-1}\right)^{j+2}}{j+2}-\dfrac{\left(x+\sqrt{x^2-1}\right)^{j}}{j} & x<-1 \quad j>0 \end{cases}, \tag{78}$$

$$\int_{-1}^{1} \sqrt{\frac{1+x'}{1-x'}} \frac{dx'}{(x-x')^2} = \pi \begin{cases} 0 & x \in [-1,1] \\ \dfrac{1}{(1-x)\sqrt{x^2-1}} & x < -1 \end{cases}, \quad (79)$$

and

$$\int_{-1}^{1} \sqrt{\frac{1+x'}{1-x'}} \ln|x-x'|dx' = -\pi \begin{cases} x + \ln 2 & x \in [-1,1] \\ x + \ln 2 - \sqrt{x^2-1} + \ln\left(-x+\sqrt{x^2-1}\right) & x < -1 \end{cases}. \quad (80)$$

In the above, T_j is the j-th order Chebyshev polynomial of the first kind

$$T_j(x) = \cos\left(j \cos^{-1} x\right). \quad (81)$$

Examples

The analysis leading to the BIEM is independent of the fan noise source description. For illustrative purposes, it is expedient to assume simplified source mechanisms with analytical expressions for the incident field. In the results presented here, a collection of N_B equally spaced point axial dipoles of unit strength located inside the duct at a radial distance $0.9r_D$ and spinning with angular speed Ω are used to simulate the loading noise produced by the fan (see figure 2). An analytical description exists for the incident field induced by this configuration[1]. The use of more sophisticated source processes is considered in the conclusion section.

To demonstrate the versatility of the BIEM, several studies were conducted for the above problem. In each study, continuous portions of the total acoustic pressure field in the unstretched, moving frame were calculated. The numerical methods described in (66-81) were implemented on a Cray YMP computer at NASA Langley Research Center. For each set of parameters considered in the studies, the computational time for both field and integral equation calculations was 2-8 minutes. The acoustic fields displayed are composed of 20,000-50,000 observer point calculations.

In the first study, $N_B = 20$ point sources with tip Mach number $M_{TIP} = 1.2$, were used to simulate the fan noise. Four forward flight Mach numbers (M_F = 0.0, 0.2, 0.4, and 0.6) were considered. Field calculations in a plane perpendicular to the fan plane and parallel to the duct axis are presented in figure 3a-d.

An examination of the pressure fields inside the duct reveals that the wavelengths of axial modes propagating in the direction of motion decreases with increasing M_F. A spectral analysis of the axial wave structure is beyond the scope of this work. However, the number of waves per unit length of the dominant axial mode present can be approximated by visual inspection. In table 1, these observations are compared to the axial wave numbers for the first radial mode from classical spinning mode theory for ducts of infinite length. If ν represents the smallest zero of the function J'_m, then the theoretical axial wave numbers are given by the formula[12]

$$k_z = \frac{\kappa}{\beta}\left[-M_F \pm \sqrt{1-\left(\frac{\nu}{\kappa}\right)^2}\right], \quad (82)$$

where J_m is the m-th order Bessel function of the first kind. Only propagating modes are considered. Note that $k_z < 0$ corresponds to axial waves traveling from the fan face to the inlet. The computed results appear to be in agreement with theory.

It is also noted that the angle between the line of peak noise and the duct axis decreases with increasing Mach number. This agrees qualitatively with the results of Rice, etal.[13].

M_F	κ	k_z (Theory)	k_z (Observed)
0.0	24.0	-1.44, +1.44	-1.5, +1.5
0.2	24.5	-2.47, +0.88	-2.5
0.4	26.2	-4.23, +0.59	-4.0
0.6	30.0	-7.59, +0.43	-7.5, +0.5

Table 1: Propagation Properties for Figure 3 Results
($M_{TIP} = 1.2 \quad L_D = 1.0 \quad m = N_B$)

Using the same source configuration as above, the effects of increasing tip Mach number for fixed flight Mach number $M_F = 0.8$ were examined (see figure 4a-d and table 2). With regard to propagation and radiation characteristics, similar comments as in the previous study apply for cases 4a and 4b.

In cases 4c-d, the waves moving forward in the duct are in agreement with the theoretical results. However, waves traveling toward the exit are present

that are not accounted for in the theory. The modified frequencies for these two cases are relatively close to some eigenfrequencies for the interior Dirichlet problem. That is, the eigenfrequencies are occurring at the zeroes of J_m. There appear to be resonant radial modes present. Condition numbers for the linear system (71) at these frequencies increase significantly. The numerical results are therefore questionable. This phenomenon has been well studied in the literature and is usually associated with ficticious interior eigenfrequencies while solving exterior problems. The interested reader is referred to the work of Kleinman and Roach[14] for a comprehensive theoretical discussion on the removal of the ficticious eigenfrequencies. In the present work, the interior is real and the eigenfrequencies are not necessarily ficticious. Research into the subject is ongoing. The authors believe that the ill conditioning can be mitigated by the use of singular value decomposition methods. We further contend that acoustic treatment of the duct interior will eliminate the problem entirely.

M_{TIP}	κ	k_z (Theory)	k_z (Observed)
0.5	16.7	none	none
0.7	23.3	-3.06, -6.84	-6.5
0.9	30.0	-1.02, -11.71	-11.5, +3.0
1.1	36.7	-4.29, -15.52	-15.0, +6.0

Table 2: Propagation Properties for Figure 4 Results
($M_F = 0.8 \quad L_D = 0.5 \quad m = N_B$)

The third example was chosen to demonstrate the capability of the BIEM to computer higher harmonics and different portions of the acoustic field (figure 5a-c). In this case, $N_B = 16$, $M_F = 0.2$, and $M_{TIP} = 1.7$. The kinematic properties and the observer locations were selected to correspond to those used for tests conducted with the Langley ducted propeller simulator[15]. Direct comparisons with the results in reference 15 are not possible because of the simplified source model used for the BIEM. The results do show, however, the ability of the BIEM to compute the sound field in regions of interest.

Conclusions

The results presented here demonstrate that the BIEM is a versatile and computationally efficient tool for predicting ducted fan engine noise. Qualitative radiation and duct propagation results can be obtained by using simplified source models such as spinning point or line sources. By tuning the strengths of the resulting monopoles and dipoles to account for fan loading and thickness effects, it is believed that the BIEM can produce results that are useful for quantitative studies.

Other boundary integral techniques have been developed for the problem of scattering of incident sound by a thin duct with hard walls[1-5]. The BIEM developed here is valid for many situations of interest and features extensive mathematical analyses on the integral equation kernels. The analyses yield expressions for singular and logarithmic integral operators that can be evaluated in terms of known functions and continuous portions that can be evaluated by simple numerical quadrature schemes. This versatility and depth of analysis, absent in the referenced works, simplify the calculations considerably.

Realistic duct geometry is included in the boundary integral equation formulation. Implementation of an arbitrary duct profile requires the solution of a system of two hypersingular integral equations. The inclusion of a duct centerbody produces another integral equation with the same properties. Both the duct profile and centerbody have interior regions that produce ficticious eigenfrequencies for the Neumann or Dirichlet boundary value problems. This difficulty can be alleviated in several ways. The method of Burton and Miller[16] appears to be adaptable to the BIEM presented here. Ficticious eigenfrequencies are not present if the engine components are acoustically lined.

The use of passive noise control techniques are included in the BIEM. A spatially varying, locally reactive liner model appears in the boundary conditions. This property makes the BIEM attractive for active and passive noise control design studies.

References

1. J. Lan: Acoustic Shielding from a Short Rigid Duct Around a Propeller, Master's Thesis, The George Washington University, August 1993.

2. J. Buhler: A New Boundary Integral Method for Predicting the Acoustic Field Generated by Ducted Rotating Sources, Master's Thesis, The George Washington University, August 1994.

3. R. Martinez: Aeroacoustic Diffraction and Dissipation by a Short Propeller Cowl in Subsonic Flight, NASA CR 190801, April 1993.

4. R. Martinez: A Boundary Integral Formulation for Thin-walled Shapes of Revolution, J. Acous. Soc. Am., 87(2), February 1990.

5. M.A. Hamdi and J.M. Ville: Development of a Sound Radiation Model for a Finite Length Duct of Arbitrary Shape, AIAA Journal, Vol. 20, No. 12, December 1982, pgs. 1687-1692.

6. M.K. Myers: On the Acoustic Boundary Condition in the Presence of Flow, Journal of Sound and Vibration, 71(3), 1980, pgs. 429-434.

7. F.D. Gakhov: Boundary Value Problems, Dover Publications, Inc., New York, 1966.

8. V.I. Smirnov: A Course of Higher Mathematics, Vol. IV, Pergamon Press, Oxford, 1964.

9. M. Golberg: The Convergence of Several Algorithms for Solving Integral Equations with Finite-Part Integrals, Journal of Integral Equations 5, 1983, pgs. 329-340.

10. F. Farassat: Introduction to Generalized Functions with Applications in Aerodynamics and Aeroacoustics, NASA TP 3428, May 1994, (Corrected Copy - February 1996)

11. A.C. Kaya and F. Erdogan: On the Solution of Integral Equations with Strongly Singular Kernels, Quarterly of Applied Mathematics, Volume XLV, Number 1, April 1987, pgs. 105-122.

12. Walter Eversman: Theoretical Models for Duct Acoustic Propagation and Radiation, Chapter 13, Aeroacoustics of Flight Vehicles: Theory and Practice, Vol. 2: Noise Control, NASA RP 1258, August 1991.

13. E.J. Rice, M.F. Heidmann, and T.G. Sofrin: Modal Propagation Angles in a Circular Duct with Flow and their relation to Sound Radiation, 17th Aerospace Sciences Meeting Paper AIAA-79-0183, New Orleans, 1979.

14. R.E. Kleinman and G.E. Roach: Boundary Integral Equations for the Three-Dimensional Helmholtz Equation, SIAM Rev., Vol. 16, No. 2, 1974.

15. R.H. Thomas, C.H. Gerhold, F. Farassat, O.L. Santa Maria, W.E. Nuckolls, and D.W. De Vilbiss : Far Field Noise of the 12 Inch Advanced Ducted Propeller Simulator, 33rd Aerospace Sciences Meeting and Exhibit Paper AIAA-95-0722, Reno, 1995.

16. A.J. Burton and G.F. Miller: The Application of Integral Equation Methods to the Numerical Solution of Some Exterior Boundary Value Problems, Proc. Roy. Soc. Ser. A, 323, 1971, pgs. 201-210.

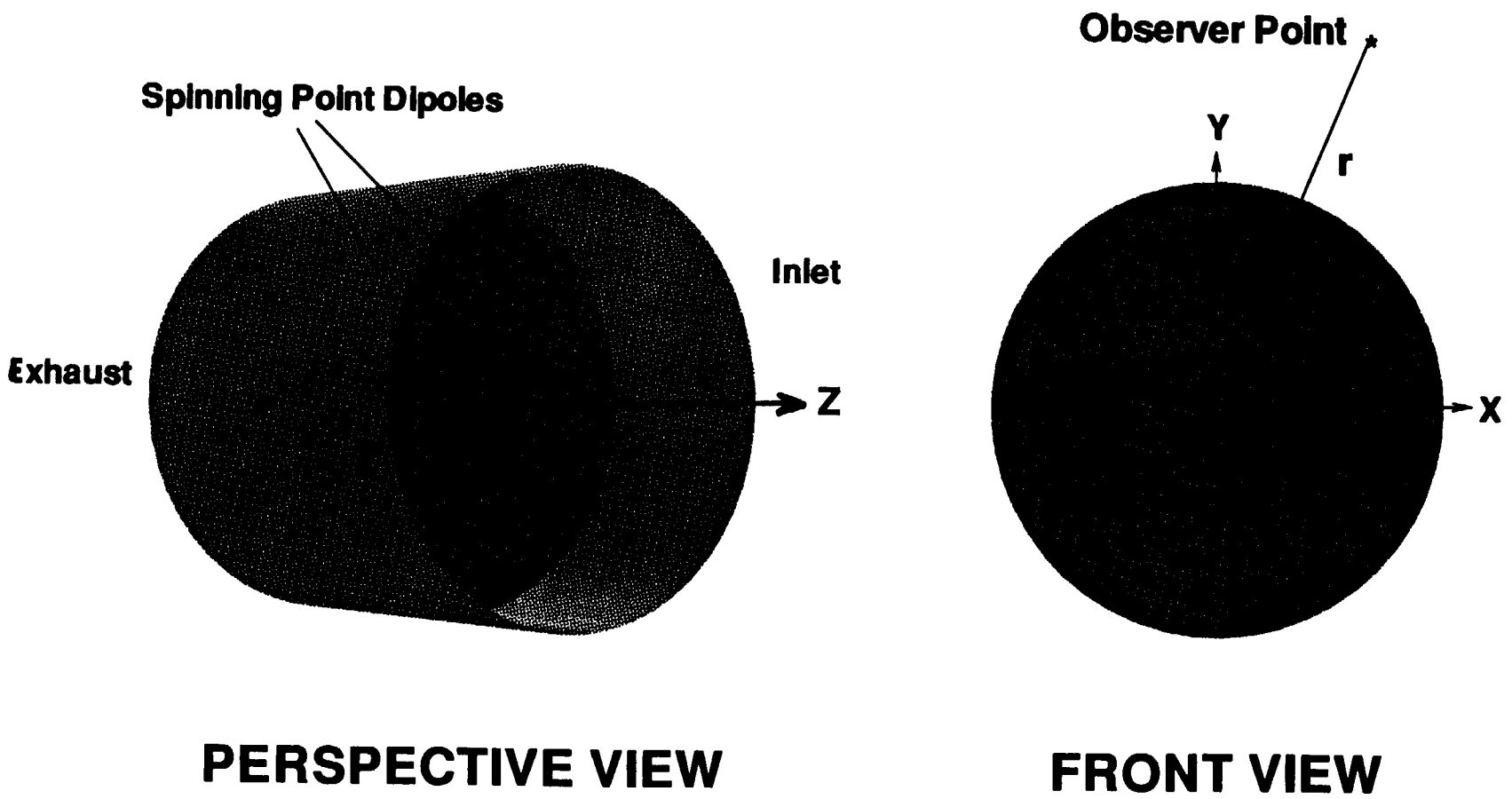

Figure 2: Geometry and Coordinate Definitions for BIEM Noise Prediction

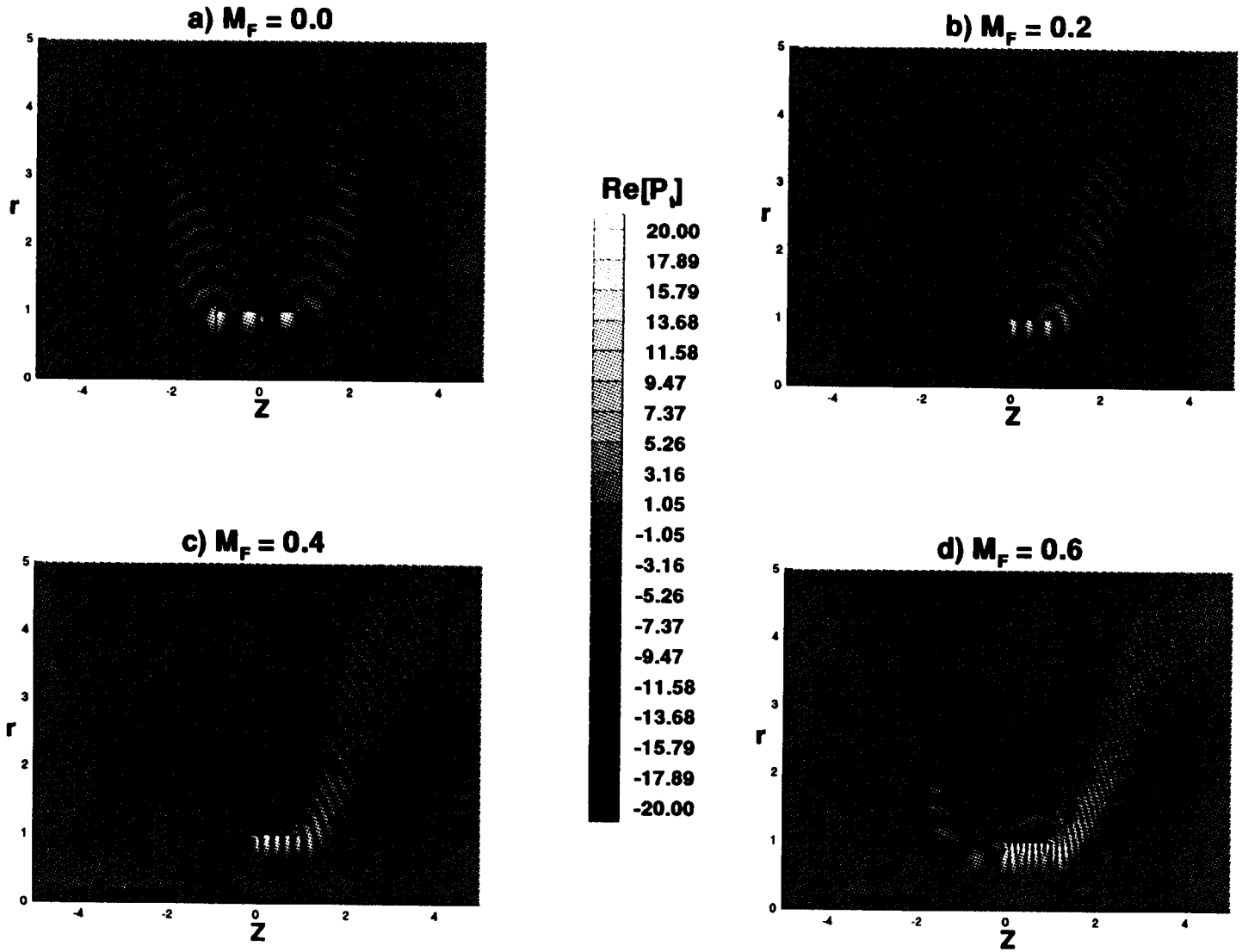

Figure 3: Total Pressure Field

$m = 20 \quad M_{TIP} = 1.2 \quad L_D = 1.0$

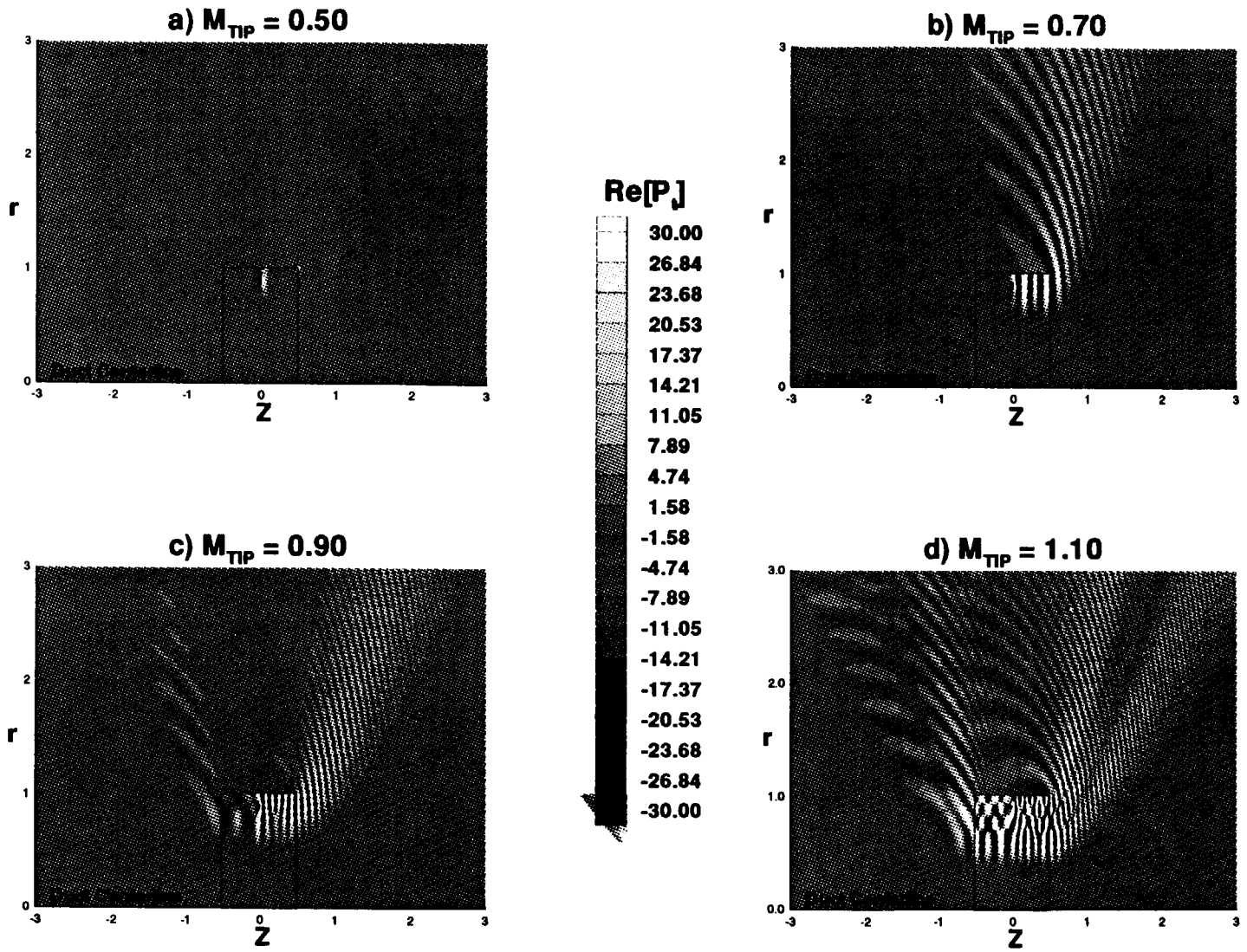

Figure 4: Total Pressure Field

$m = 20 \quad M_F = 0.8 \quad L_D = 0.5$

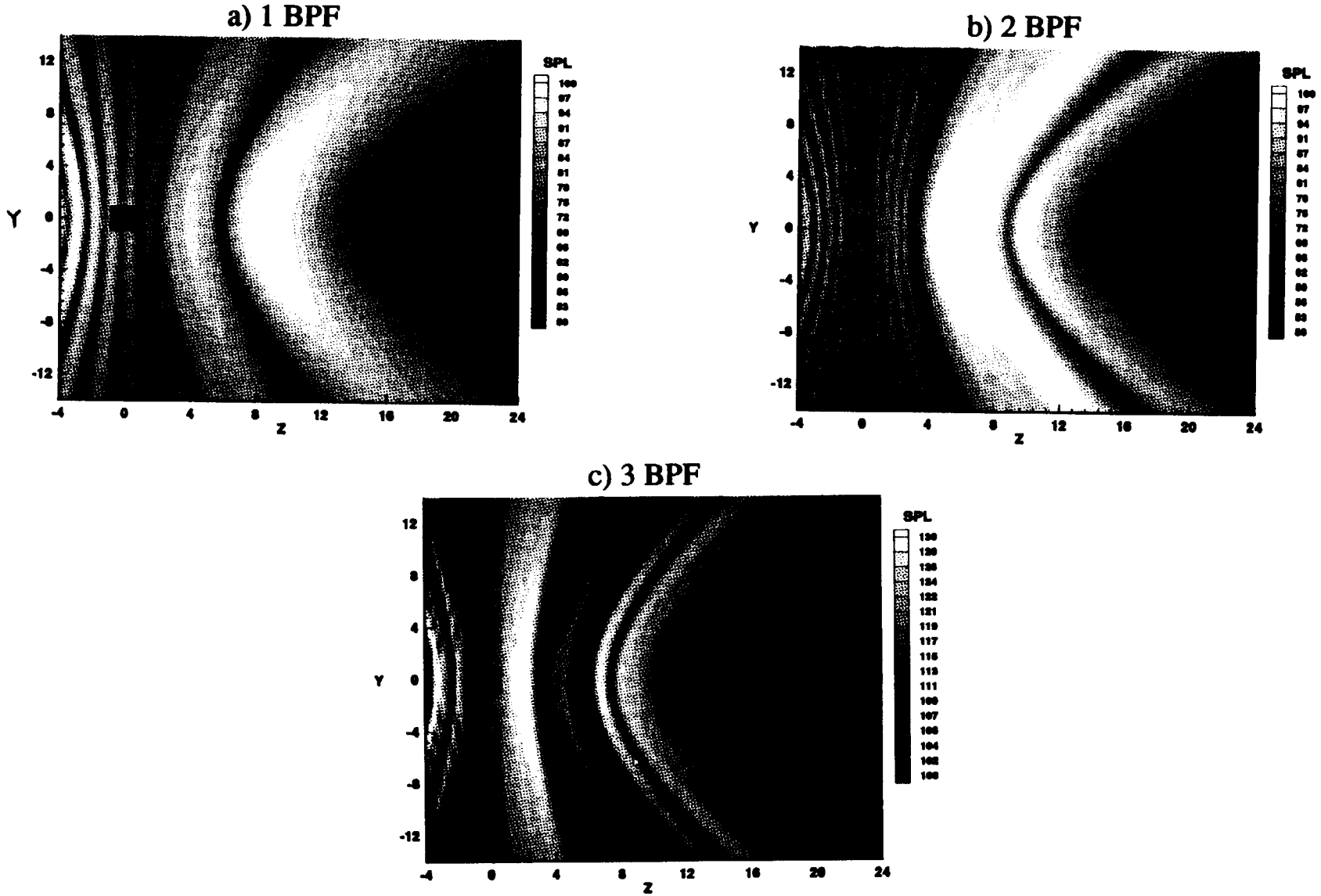

Figure 5: Noise Footprint for Langley Ducted Fan Rig

$N_B = 16 \quad M_F = 0.2 \quad M_{TIP} = 1.7$